Graphical abstract

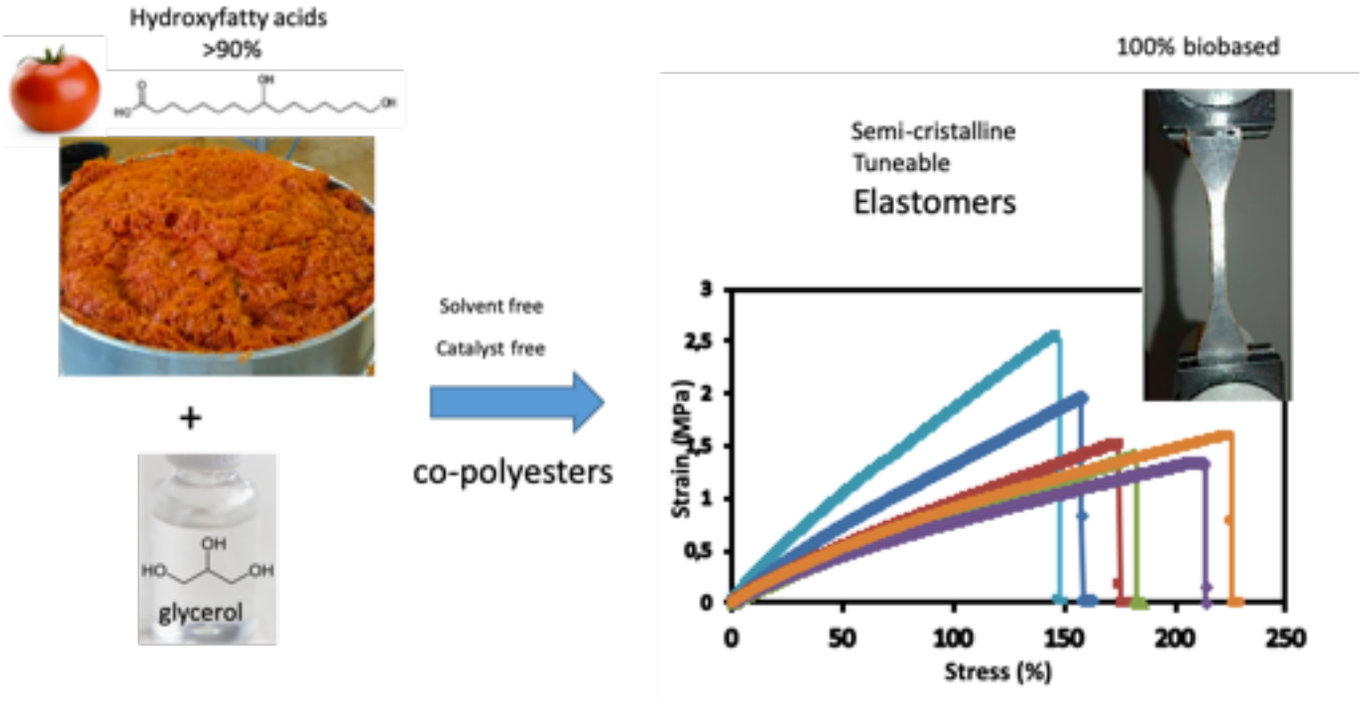

1

2

Bioinspired co-polyesters of hydroxy-fatty acids extracted from tomato peel agro-wastes and glycerol with tunable mechanical, thermal and barrier properties

Mathilde Marc[†], Regis Risani[†], Eric Desnoes[†], Xavier Falourd[†,¶], Bruno Pontoire[†], Rúben Rodrigues[&], Rita Escórcio[&] , Ana Paula Batista[‡], Romain Valentin[§], Nathalie Gontard[‡], Cristina Silva Pereira[&], Christelle Lopez[†], Eric Leroy[¦], Denis Lourdin[†], Didier Marion[†], Bénédicte Bakan[†*].

[†] Biopolymers Interactions Assemblies Research Unit 1268 (BIA), INRAE, Rue de la Géraudière, 44316, Nantes, France

[‡] Agropolymers Engeneering and Emerging Technologies Joint Research Unit 1208 (IATE), INRAE-CIRAD-SupAgro-University of Montpellier, 2 place Viala, Montpellier, 34000, France

[§]Agro-Industrial Chemistry Joint Research Unit 1010 (LCA), INRAE-INP-ENSIACET, 4 Allée Emile Monso, Toulouse, 31000, France

[¶]Biopolymers and Structural Biology platform (BIBS), BIA research unit, INRAE, rue de la Géraudière, Nantes, 44300, France

[¦]Université de Nantes. Oniris. CNRS. GEPEA. UMR 6144, 44600 Saint Nazaire, France.

[&] Instituto de Tecnologia Química e Biológica António Xavier, Universidade Nova de Lisboa (ITQB NOVA), Av. da República, Oeiras, 2780-157, Portugal.

*corresponding author: benedicte.bakan@inrae.fr

Highlights

- High yield extraction process enables recovering unique fatty acids from cutin-rich agro-industrial byproducts.
- Polyesters biobased and bioinspired by native cutin are synthesized by co-polymerization of fatty acid extracts and glycerol
- Tuning the amount of esterified glycerol induced modification in the macromolecular structure and crystallinity.
- Resulting modified properties comprise elastomer like mechanical behavior (with up to 200% elongation), a decrease in O_2 permeability, and an increase in anti-biofouling properties

Abstract

By mimicking the cutin natural polyester networks of plant cuticles, we produced hydrophobic elastomers by a sustainable process, i.e., using a catalyst- and solvent-free polycondensation of glycerol and hydroxy fatty acids, two by-products of the agro-food industry. The hydroxy fatty acid fraction was obtained by ethanolic alkaline hydrolysis of cuticle from industrial tomato. This industrial-like fatty acid fraction contained more than 90% wt. of 9(10)-16 dihydroxyhexadecanoic acid (diOHC16). The co-polyesters were designed by increasing the ratio of esterified glycerol/diOHC16 in a range observed in plant cutins (up to 6% wt.). Their structure and functional properties (thermal, mechanical, gas permeability, interaction with bacterial cells) were characterized. Increasing the glycerol contents induced a significant decrease in the crosslink density of the polyesters and the formation of crystalline domains with a hexagonal organization. These structural modifications were related to a marked increase of elastomeric extensibility (up to 217%). While water vapor permeability was not impacted, the increase of glycerol content induced a significant decrease in oxygen permeability. None of the polyesters displayed biocide activity, but an increase of glycerol content significantly reduced the adhesion of bacterial cells, potentially giving rise to antifouling applications.

Keywords

Tomato cuticle, biomimetic, cutin polyester, hydroxy fatty acid, glycerol, semi-crystalline elastomer

1. Introduction

To face terrestrial life colonization, plants have developed a hydrophobic barrier, the cuticle, that covers the surface of their aerial organ. This ubiquitous interface between the plant and its environment fulfills multiple crucial functions such as mechanical supports against wounding and cracks, control of non-stomatal water loss, and permeation of gases (Fich et al., 2016).

The main biopolymer in this complex hydrophobic assembly is the cutin polyester, which is essential for the functional properties of the plant cuticle (Nawrath, 2006; Yeats and Rose, 2013). Plant cutin is insoluble due to its polyester network architecture. It can be depolymerized mainly into a variety of long-chain hydroxy fatty acids building blocks. Each of these carboxylic acid monomers contains 16 and-or 18 carbon atoms and one to three hydroxyl groups. Interestingly, the tomato fruit peels concentrate a high amount of cutin, whose monomer composition is strikingly homogenous, with about 80% by weight consisting of 9(10)-16 dihydroxyhexadecanoic acid (diOHC16). The remaining minor cutin components, especially phenolics, mono- and di-carboxylic acids probably play an important role in the insoluble polyester crosslinked network. Indeed, pure diOHC16 is an AB2 type molecule (with A being a carboxylic acid function and B a hydroxyl group). The polyesterification of such a single monomer would typically lead to hyperbranched macromolecules that are easily soluble in common organic solvents (Feast and Stainton, 1995; Testud et al., 2017).

However, this ω-hydroxylated molecule carrying midchain functionalities, presents high interfacial properties (Fameau et al., 2013) and constitutes a unique opportunity for the development of innovative biosourced polymer materials from depolymerized tomato cutin feedstock (Heredia-Guerrero et al., 2017). Reaching this innovation would address the important landmarks set by the United Nations sustainable development goals because tomato cutin is a readily available residue of the tomato processing industries.

Tomato wastes, i.e., pomaces, are mainly composed of peels and seeds. 44 MT of tomato fruit are processed worldwide, to make derived tomato products (e.g., purees, juice, sauces) generating nearly 1.5 MT of animal feed and production of biogas whereas their transformation for development of new materials, from bioplastic to high-functional value products remains largely overlooked (Fritsch et al., 2017). Peels and seeds can be easily separated and dried, directly in the factory, and the hydroxy fatty acids can be easily extracted from the cutin of tomato peels (Benítez et al., 2018).

Furthermore, glycerol, the main by-product of the biodiesel and oil industries (Quispe et al., 2013), has been identified as a potentially influential minor component in tomato cutin. Esterified glycerol has been evidenced in the cutin polyester network structure (Graça et al., 2002) and typically represents only 0.6 to 0.7 % wt. of the cutin monomers obtained by depolymerization (Philippe et al., 2016). Besides, we have recently highlighted that the ratio of glycerol to hydroxy fatty acid can be modulated in tomato fruit. Indeed, in tomato fruit mutants affected in a cutin synthase (CUS1), an enzyme involved in the cutin biosynthesis, a 60% reduction in cutin deposition was induced without any significant negative impact either on the fruit development or the generation of cracks (Girard et al., 2012). Looking at the cutin polyester structure, we observed a significant increase of the glycerol to hydroxy fatty acid ratio. These results obtained with the mutants suggested that the inclusion of co-polymerized glycerol in the tomato cutin network could be involved in the mechanical adaptation of the fruit cuticle, in particular in the modulation of its extensibility. This is especially essential for resistance to turgor pressure during fruit growth and environmental constraints to prevent fruit from cracking, a phenomenon responsible for major crop losses (Barker, 1988). Taking inspiration from nature, our leading hypothesis is that we can produce tunable bio-based co-polyesters that mimic potential adaptive events of cutin simply by playing on the glycerol/diOHC16 ratio.

Hereinafter, we describe a solvent- and catalyst-free polymerization process to generate co-polyesters from two diOHC16 and glycerol, two readily available and renewable biological resources. Tuning of the ratio of esterified glycerol to diOHC16 in a range similar to what it is observed in plant cutin effectively results in the modulation of the structure (amorphous or semi-crystalline), the properties (mechanical, thermal, and barrier properties) of the ensuing co-polyesters.

2. Experimental Section

2.1. Materials

Glycerol (99 % purity) and all other chemical ACS reagents were from Sigma-Aldrich (USA). The analytical grade solvents were obtained from Carlo Erba (Val de Reuil, France). The 16-10(9)-hydroxy-hexadecanoic acid-enriched fraction (referred to as "diOHC16" in the manuscript) was extracted from industrial tomato samples provided by the "Conserveries de Bergerac" (UNIPROLEDI, Bergerac, France). The peels and seeds of the pomaces were separated by decantation in a water tank. The floating peels were recovered, their water excess was squeezed out and then dried at room temperature. Dried peels (1kg) were grounded and dewaxed under the reflux of acetone: ethanol 1:1 (v:v) in a Soxhlet extractor and then dried in a fume hood. Cutin depolymerization was conducted at room temperature in 5% (wt.) KOH in ethanol 95%. After filtration on a Buchner funnel, about 90% of the filtrate was evaporated under vacuum and replaced by water. Hydroxy fatty acids were precipitated by adjusting pH at 3.5 with concentrated HCl. The hydroxy fatty acid precipitate was extensively washed with water, and finally freeze-dried.

The purity of the fatty acids was determined after phase partitioning in $CHCl_3/CH_3OH/H_2O$ 8:4:3 (v:v). The lower chloroform-rich phase containing only lipophilic compounds, mainly fatty acids and some pigments, was recovered, evaporated under vacuum, and weighed. The colored cutin monomer batches

contain 98 ± 0.5% of lipophilic compounds. The fatty acid composition of the lipophilic fraction was determined by gas chromatography coupled to a mass spectrometer as previously described (Philippe et al., 2020). A 60% yield of hydroxy fatty acids was obtained and the same batch of 500g of diOHC16 extract was used in the study. This batch was dark-red colored due to the remaining pigments and highly concentrated in diOHC16 (90% of the hydroxy fatty acids) (**Supplemental Figure 1**).

2.2. Preparation of the cutin-like co-polyesters films

Co-polyesters films were produced by a solvent-free and catalyst-free polycondensation. We developed a polymerization process to minimize the non-esterified glycerol within the copolyester films. Preparation of different weight ratio of diOHC16/ Glycerol (1.8g diOHC16 for PG0 ; 1.71g diOHC16/90 mg glycerol for PG2.3; 1.62gdiOHC16/180 mg glycerol for PG3.9; 1.53g diOHC16/ 270 mg glycerol for PG4.8 ; 1.44g diOHC16/ 360 mg glycerol for PG5.2 and 1.35 g of diOHC16/ 450 mg glycerol for PG6.2 respectively) were put in Teflon molds (5cm x 5cm) with a thickness of about 0.7-1 mm. The nomenclature of the co-polyesters refers to the glycerol weight ratio comprised within the co-polyester at the end of the process (**Table 1**). Bulk poly-condensation was then conducted for 24h at 150°C in an oven (VaccuTherm, ThermoFisher, USA). To avoid bubbles and to minimize the presence of residual free glycerol, i.e., non-esterified, in the final material a 400mbar vacuum was applied during the first 2h of the polycondensation process. After 24h, the polymers were rapidly cooled on ice and stored at room temperature. Samples of the ensuing films were immersed under agitation in various solvents of diOHC16 and/or of glycerol, i.e., water, ethanol, and chloroform 16h at room temperature to assess their solubility.

2.3. Structural characterization of the cutin-like co-polyester films

Attenuated total reflectance Fourier-transform infrared spectroscopy (ATR-FTIR) spectra (200 scans) were recorded at a resolution of 2 cm^{-1} on a Nicolet Magna IR 550 spectrometer equipped with a liquid nitrogen-cooled mercury−cadmium−telluride detector. The instrument was continuously purged with dry air. Spectra of co-polyester films were obtained by attenuated total reflection (ATR) using a single reflection accessory fitted with a thermostated diamond crystal with a 45° angle of light incidence. All spectra (3 per co-polyester) were acquired in the 4000 to 700 cm^{-1} range at 4cm^{-1} resolution and accumulating 30 scans.

^{13}C solid-state NMR (CP-MAS NMR) was carried out on a Bruker AvanceIII-400 MHz spectrometer operating at 100.61 MHz for ^{13}C, equipped with a double-resonance H/X CP-MAS 4-mm probe for CP-MAS (cross-polarization magic-angle-spinning) solid-state experiments. Sixty mg of the co-polyester films were put packed into 4 mm zirconia rotors. The samples were spun at 12,000 Hz at room temperature. CP-MAS spectra were acquired with a contact time of 1 ms, a recycling delay of 10 s, and over-accumulation of 2048 scans. The carbonyl carbon was set to 176.03 ppm through external glycine calibration. NMR spectra deconvolution was performed using the PeakFit® software (Systat Software, Inc., USA).

X-Ray Diffraction analysis was performed on a Bruker-AXS D8 Discover diffractometer. The X-ray beam was produced in a sealed copper tube at 40 kV and 40 mA. The 500-µm beam with a CuKα1 wavelength (1.5405 Å) was collimated and parallelized using two crossed-coupled Göbel mirrors. The X-ray diffraction data were collected using a Vantec500 two-dimensional detector, previously calibrated with silver behenate, in the 2.θ-range: 3-70°. The samples are placed perpendicular to the X-ray beam. Recorded diffractograms I = f (2θ) were normalized to remove the influence of thickness variation among the samples. Temperature kinetics were performed using Linkam's HFS91 stage. The samples were placed in a mica window cell. The detector was positioned at a focusing distance of 8.6 cm from the sample surface.

It was in a direct beam position. The heating kinetic applied to the sample was 3°C.min^{-1} from 20°C to 100°C.

2.4. Chemical characterization of the cutin-like co-polyester films

Free glycerol was extracted from polymers (5mg in 1 mL of CH_3OH), overnight at room temperature. Esterified glycerol was released from polymers by mild methanolysis using a modified procedure (Graça et al., 2002). Isolated pieces of the co-polyester films were stirred at room temperature in a mixture of 50mM sodium methoxide in dry methanol with the internal standard 1,2,3-butanetriol (Shen and Xu, 2013). Free and esterified glycerol extracts were dried with a nitrogen flow and analyzed by GC-MS and GC FID. For the quantification of the cutin hydroxy fatty acids, the co-polyesters were depolymerized through methanolysis during 6h until complete depolymerization. The depolymerized hydroxy fatty acids were silylated with 1% BSTFA/TMCS and analyzed by GC-MS and GC-FID as previously described (Philippe et al., 2016).

Free OH groups were derivatized by benzyl-etherification resistant to alkaline depolymerization, according to an established method (Philippe et al., 2016). Briefly, co-polyesters (3mg) were mixed at 90°C in a screw-capped glass tube for 24h with 15mg of 2-benzyloxy-1-methylpyridinium triflate and 1.68 mg of magnesium oxide in 1mL of trifluorotoluene. The samples were then extensively washed with CH_2Cl_2 and dried before depolymerization and cutin monomer analysis. GC-FID surface response of the llabeleddiOHC16 (either in midchain position or in $\omega-$position) were compared between the different co-polyesters and were expressed as equivalent of heptadecanoic acid, as an external standard.

2.5. Thermal and mechanical properties of the cutin-*like* co-polyester films

189 Differential Scanning Calorimetry (DSC) was performed on a DSC Q100 (TA Instruments, New Castle, DE,
190 USA). The DSC instrument was calibrated with an indium standard. Analyses were made with 2–5mg of
191 samples, using hermetically-sealed aluminum pans. An empty pan was used as a reference. Samples were
192 cooled from 20°C to −50°C and heated at 3°C.min^{-1} until 80°C. The Glass transition temperature (Tg) of the
193 co-polyesters was defined at the midpoint of heat capacity change on the thermograms recorded on the
194 first scan. The melting temperature was determined at the maximum of the peak.

195 Dynamic Mechanical Thermal Analysis (DMTA) was performed on a DMTA MKIV (Rheometric
196 Scientific, US). Rectangular specimens (20 mm × 4 mm) were cut from the films and thickness of about 0.7-
197 1 mm was precisely measured with a micrometer. The samples were analyzed in the tensile mode at the
198 frequency of 1 Hz with a strain amplitude of 0.1%. To keep the samples taut a static force superior by 10%
199 to the dynamic force was applied to the sample. A scanning rate of 3°C min^{-1} from -50°C to 80 °C was used.
200 Each sample was analyzed in duplicate.

201 The tensile test of the films was carried out using MTS Synergie 100 (MTS Systems Corporation,
202 USA). The film samples were cut into a dog-bone shape. The test was performed using a cross-head speed
203 of 10 mm/min. The reported results, including Young's modulus, ultimate strength, and elongation at
204 break, were the average values of five specimens. The standard deviations are indicated in **Table 1**.
205

206 **2.6. Barrier properties of the cutin-like co-polyester films**

207 Water permeances of the co-polyesters were determined at 25°C and under 100% relative humidity
208 gradient using transpiration chambers as previously described (Philippe et al., 2016; Schreiber L and J,
209 2009). Typically, co-polyesters (5 replicates) were mounted on the top of the transpiration chamber with
210 a 0.6 cm diameter hole, subsequently filled with 300 µL of deionized water, inverted, and placed in a

desiccator filled with a desiccant. Water transfer across the co-polyesters samples was determined by gravimetric analysis of the transpiration chamber every 8h during 4 days. Water permeance (P) was calculated as the ratio P=F/A.Δc, where F (Flow rate of water) is determined as the slope of water transfer across the samples (in $g.s^{-1}$), A (in m^2) is the area across which transport has occurred, and Δc (in $g.m^{-3}$) is the water gradient driving force.

The oxygen permeability of co-polyesters was determined in triplicate at 23°C and 0% relative humidity through an isostatic and dynamic method using gas-phase chromatography as previously described (Motedayen et al., 2019). The film samples (4 cm diameter) were placed inside sealed stainless-steel permeability cells. The lower chamber was continuously spread by a 5 $mL.min^{-1}$ flux of permeant gas (O_2), and the upper chambers by the same flux of vector gas (helium), thus applying a permanent O_2 partial pressure difference. The permeability cells were coupled to a gas chromatograph with a thermal conductivity detector (GC-TCD, Agilent 7890A, USA), equipped with an automatic valve to online analyze the evolution with time of O_2 gas concentration in the upper chamber. The GC-TCD was equipped with two capillary columns - PoraPlot U (25 m × 0.530 mm id, Agilent) and HP Molesieve (30 m × 0.535 mm id, Agilent) – able to separate O_2, CO_2 and N_2. Data were collected and processed using the ChemStation OpenLab Software (Agilent) and SRA Prochem interface (SRA Instruments). The O_2 permeability, P_{O2} ($mol.m^{-1}.s^{-1}.Pa^{-1}$), of the film samples was calculated as follows:

$$P_{O_2} = \frac{J \times e}{A \times \Delta P} \qquad \text{(equation1)}$$

Where: J ($mol.s^{-1}$) is the flux of gas that passes through the film, e is the film thickness (m), A is the permeation area (m^2) and ΔP is the O_2 pressure differential between the upper and lower chambers of the cell (Pa).

2.7. Microbiological analyses

S. aureus NCTC8325 and *E. coli* TOP 10 cells (10^5 cells·mL^{-1}) in Mueller-Hinton broth (MHB) medium were exposed for 24h to 0.5 cm^2 of polyester films (*ca.* 10 to 20 mg·mL^{-1}) at 37 °C, under orbital agitation (100 rpm). Upon incubation, the cellular morphology and the viability of the bacterial cells were visualized by light and fluorescent microscopy, respectively, using a Leica DM6000 B microscope equipped with an iXon EM+ 885 EMCCD camera (Andor Technology®). The fluorescent dye propidium iodide (PI) was used for labeling the dead cells (red fluorescence). Negative controls, i.e., bacteria growing in media devoid of cutin-like co-polyester films, were also carried out. Films from each tested condition were also collected to scan for the presence of bacterial cells on the film's surface. All assays were done in triplicate. The films were first washed with phosphate-buffered saline (PBS) to remove non-adherent bacteria, subsequently fixed with glutaraldehyde 2.5% (v/v) during 10 min. After 10 min, samples were rinsed with distilled water and dehydrated with aqueous solutions with increasing concentrations of ethanol (ranging from 70 to 100%). Scanning electron microscopy (SEM) (microscope JEOL JSM-7001F, with an accelerating voltage set to 15 kV) was used to scan the co-polyester film's surfaces. All samples were coated with gold before analysis.

3. Results and Discussion

3.1. Sustainable production of dark black colored insoluble co-polyesters with different ratio of esterified-glycerol

The cutin-like polyesters were manufactured to meet green chemistry and sustainability criteria**.** Indeed, they were prepared through a catalyst- and solvent-free process using hydroxy fatty acids and glycerol from renewable resources, i.e. by-products of the tomato and oilseed processing industries. The biorefinery process designed for the recovery ion of the hydroxy fatty acids from tomato pomaces leads

to higher yield and purity than the existing processes described in the literature (Benítez et al., 2018; Cogognigni et al., 2014). First, fractionation of tomato pomaces into seeds and peels was conducted. This opens ways for the valorization of both seeds and peels and prevents seed lipids co-extraction. Indeed, seeds contain more than 30% oil (Giannelos el., 2005). In contrast with previous studies starting from raw pomaces, the extraction of fatty acids from peels provided a fatty acid fraction with a higher diOHC16 content (90% instead of 45% (Tedeschi et al., 2018). The hydrolytic process of the tomato cutin polyester was conducted at room temperature and used green solvents, i.e., water and ethanol, which can be recycled to improve the sustainability of the process. Interestingly, the ethanolic alkaline hydrolysis at room temperature gave rise to a high fatty acid yield (around 60% wt. of dry peels), instead of around 15% wt. for hot aqueous alkaline hydrolysis (Cogognigni et al., 2014), thereby strengthening the sustainability of the process. Considering that tomato cuticle contains about 70% of cutin and 30% of polysaccharides (Philippe et al., 2020), this means that our biorefinery process recovered more than 85% of the available cutin monomers in the tomato pomaces.

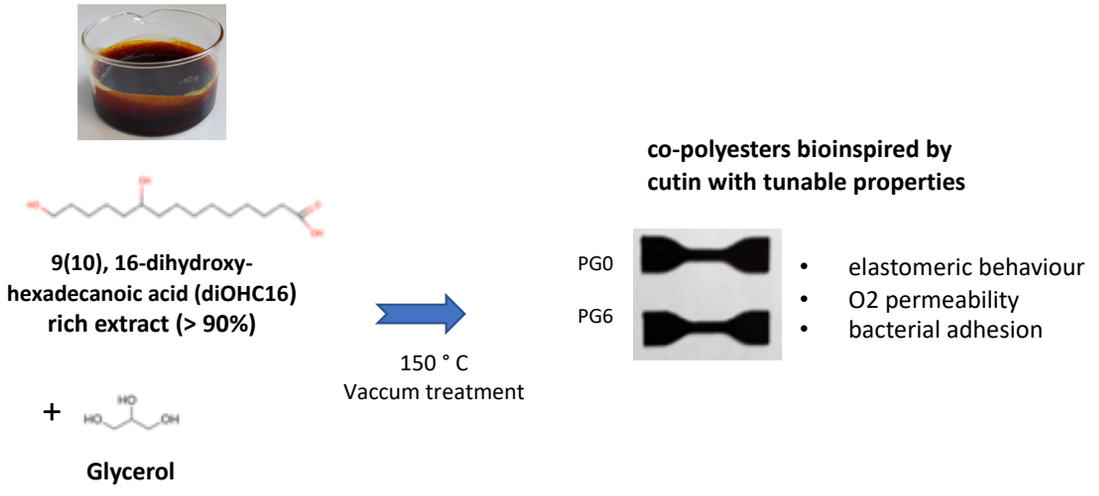

Figure 1 – Solvent- and catalyze-free polycondensation of tomato cutin extract and glycerol

The cutin monomers extract consisted of ~90 % diOHC16 and were dark-red colored as for existing processes (Benítez et al., 2018) due to the remaining pigments. According to the FTIR and UV spectra, these pigments contain phenolic compounds(Aleixandre-Tudo and du Toit, 2018; Benítez et al., 2018; Heredia-Guerrero et al., 2014; Herrera et al., 1998) (supplemental Figure 1). The cutin-like co-polyesters formed by polycondensation of the diOHC16-rich hydroxy fatty acid extract and glycerol **(Figure 1)** displayed a dark brown color. They were insoluble in water, ethanol, and chloroform **(Table 1**) as previously reported for polyesters synthesized from lower purity tomato hydroxy fatty acids extracts (Benítez et al., 2018; Benitez et al., 2015). The cutin monomers extracts were highly rich in lipophilic compounds (98%). Accordingly, the insolubility of our films suggests that, as in native plant cutin, the minor lipidic compounds, i.e., dicarboxylic fatty acids, and co-extracted phenolic molecules (supplemental Figure 1) could participate in the polymerization process. The participation of these compounds in the polyester crosslinked network should compensate for the AB2 structure of the diOHC16 which should normally lead to branched polymers soluble in organic solvents (Feast and Stainton, 1995; Testud et al., 2017).

In previous works on fatty acid extracts containing 9,10,16-trihydroxypalmitic or 9,10-dihydroxystearic acids (Benitez et al., 2015), the authors pointed out the capacity of such molecules to form two additional carboxylic acid functions by an oxidative diol cleavage reaction of the 9,10 neighbor hydroxyl groups. This would increase the acid/hydroxyl ratio and allow the formation of crosslinked insoluble polyester networks. In our case, despite oxidation reactions evidenced by the darkening that occurs during the polymerization process **(Figure 1),** no such fatty acids with vicinal hydroxyl groups are present in the diOHC16-rich extract **(supplemental Figure 1)**.

Finally, the objective of the present study was to focus on the modulating effect of glycerol on the properties of the co-polyesters produced from the fatty acid extract from peels provided by tomato

pomaces, in line with a vision of sustainable biobased and cutin-inspired chemistry. Therefore, the same cutin monomer batch was used and materials containing different amounts of esterified glycerol were produced. After the poly-condensation reaction, the added glycerol can be (i) free, i.e., non-esterified, acting as an external plasticizer, or (ii) esterified, constituting a polyester monomer. Determination of free and esterified glycerol contents revealed that more than 95% of the glycerol was esterified (**Table 1**).

W water, CF chloroform, Et Ethanol

Table 1 Composition, chemical, thermal and mechanical characterization of the cutin-inspired co-polyesters

Sample	Chemical characterisation						DSC					DMTA		Mechanical test		
	glycerol total (%wt)	esterified glycerol (% wt)	free glycerol (% wt)	Insoluble fraction (%) W	Insoluble fraction (%) CF	Insoluble fraction (%) Et	Glass transition temperature (°C)	Melting temperature 1 (°C)	Melting Enthalpy (J/g)	Melting temperature 2 (°C)	Melting Enthalpy (J/g)	Mechanical relaxation temperature (°C)	Storage Modulus at 50°C (MPa)	Breaking stress (MPa)	Strain at break (%)	Young's modulus (Mpa)
PG0.4	0.43 ±0.24	0.38 ± 0.21	0.05 ± 0.04	100	100	98	-8.7	-	-	-	-	8.6	5.867	2.1 ± 0.5	124.0 ± 24.5	2.29 ± 0.05
PG2.3	2.27 ±0.31	2.17 ± 0.32	0.10 ± 0,03	99	100	98	-13.1	-	-	-	-	5.4	5.035	2.0 ± 0.2	155 ± 12.7	1.74 ± 0.06
PG3.9	3.93 ± 0.34	3.75 ± 0.31	0.18 ± 0,05	99	99	94	-15.7	-	-	39.7	0.07	3.2	4.058	1.7 ± 0.2	180.7 ± 10.3	1.26 ± 0.2
PG4.8	4.80 ± 0.82	4.57 ± 0.80	0.23 ± 0.15	99	97	95	-17.0	17.9	0.32	41.6	2.60	1.9	1.408	1.4 ± 0.1	178.4 ± 8.6	1.11 ± 0.03
PG5.2	5.20 ± 0.31	4.87 ± 0.5	0.32 ± 0.2	99	94	91	-20.4	16.8	2.04	41.2	7.96	0.9	1.521	1.3 ± 0.1	197.3 ± 21.1	1.10 ± 0.01
PG6.2	6.18 ± 0.39	5.89 ± 0.45	0.29 ± 0.1	100	88	80	-18.5	18.3	0.59	41,6	9.05	0.2	1.589	1.5 ± 0.1	217.6 ± 14.2	1.19 ± 0.08

3.2. A gradual increase of the glycerol content induces a decrease in the branching of the co-polyester films

The co-polyesters containing the lowest (PG0.4) and the highest (PG6.2) levels of esterified glycerol were characterized by ATR- FTIR and ^{13}C NMR (**Figure 2**). ATR-FTIR indicated the formation of esters bonds in these co-polyesters. Indeed, we observed the characteristic shift of the carbonyl band from 1705 cm^{-1}, assigned to the carboxylic acid, to the 1733 cm^{-1} band assigned to the esterified carbonyl(Heredia-Guerrero et al., 2014). In addition, the 1715 cm^{-1} band assigned to the ester bond involved in hydrogen bonding was also evidenced, as previously observed in tomato cutin (Girard et al., 2012). In our present co-polyesters, the hydrogen bonds could involve the free hydroxyl groups either from the hydroxy fatty acids and/or from the esterified glycerol. Besides, the 1171 cm^{-1} band assigned to the stretching vibration of the C-O-C ester bond was observed in all co-polyesters. Likewise, the ^{13}C C-MAS (**Figure 2B**) data confirmed the formation of esters, evidenced by a single broad peak at 173 ppm and by the peak at 64 ppm, which is assigned to primary esters (Tedeschi et al., 2018). Furthermore, no significant free fatty acid signals were evidenced at 178 ppm (-COOH) and 35 ppm (-CH_2-COOH). Finally, the comparison of the surface ratio of the 33.7 ppm and 37 ppm peaks, assigned to aliphatic carbons (-CH_2-CHOR-CH_2-) and (CH_2-CHOH-CH_2) respectively (Benitez et al., 2015), indicated a decrease (40%) in the esterification of the secondary hydroxyls of diOHC16 associated with the increase in the glycerol content.

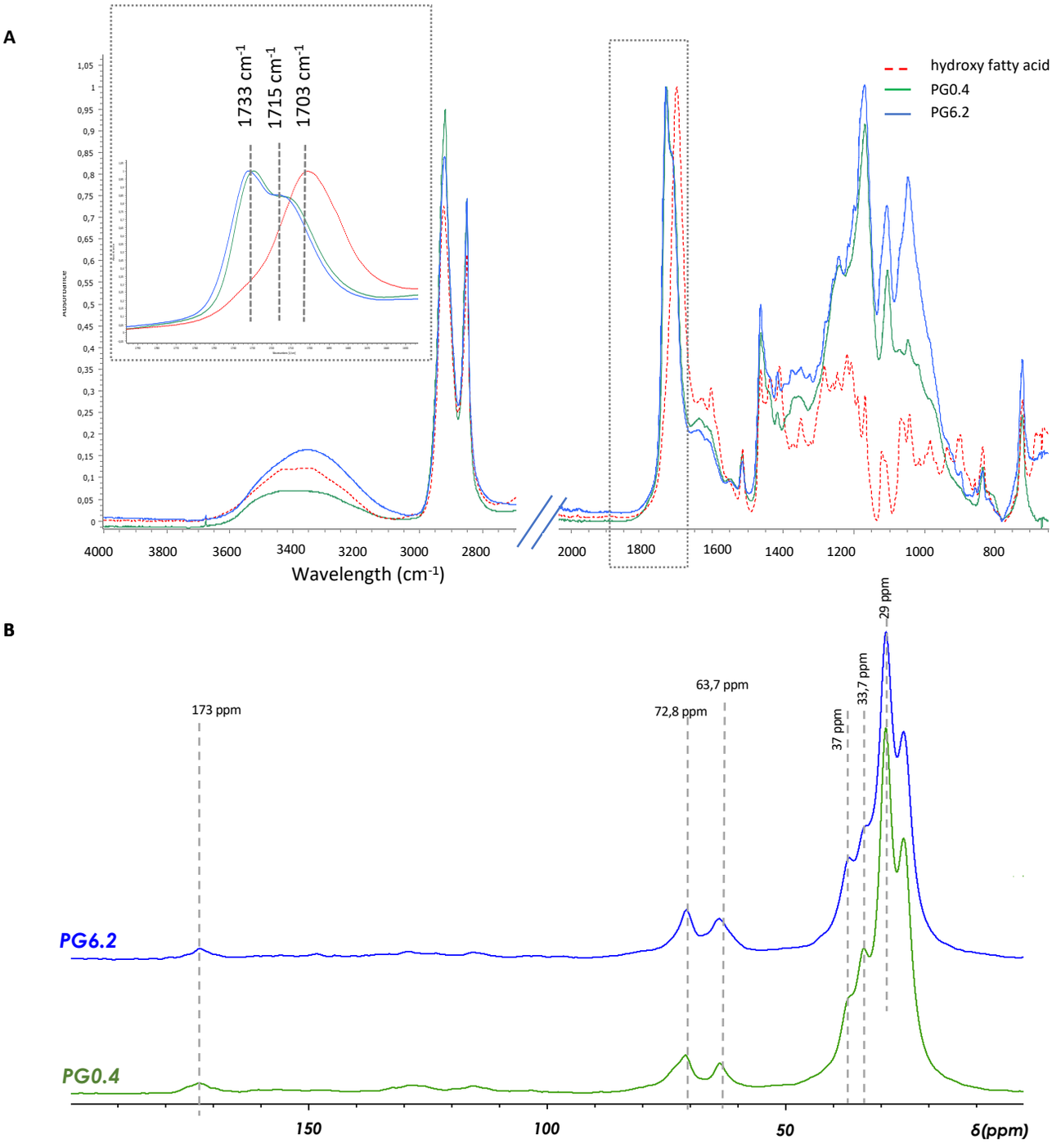

Figure 2- ATR-FTIR and NMR spectra of the cutin-like polyesters films

A . ATR-FTIR spectra of hydroxy-fatty acid (diOHC16) extracted from tomato cutin and the corresponding polymers with high (PG6.2) or low (PG0.4) glycerol. In inset, the magnification of the CO streching bands at 1733 cm^{-1} and 1715 cm^{-1} are assigned respectively to ester group, and ester bond interacting by hydrogen bond whereas the band at 1703 cm^{-1} is assigned to carboxylic group.

B. Solid State ^{13}C CP-MAS NMR spectra of the polymers

314

315 The reticulation of the co-polyesters was further monitored by the chemical labeling of the free OH
316 groups by benzyl ether within the diOHC16-derived polyesters (Philippe et al., 2016) (**Figure 3**).

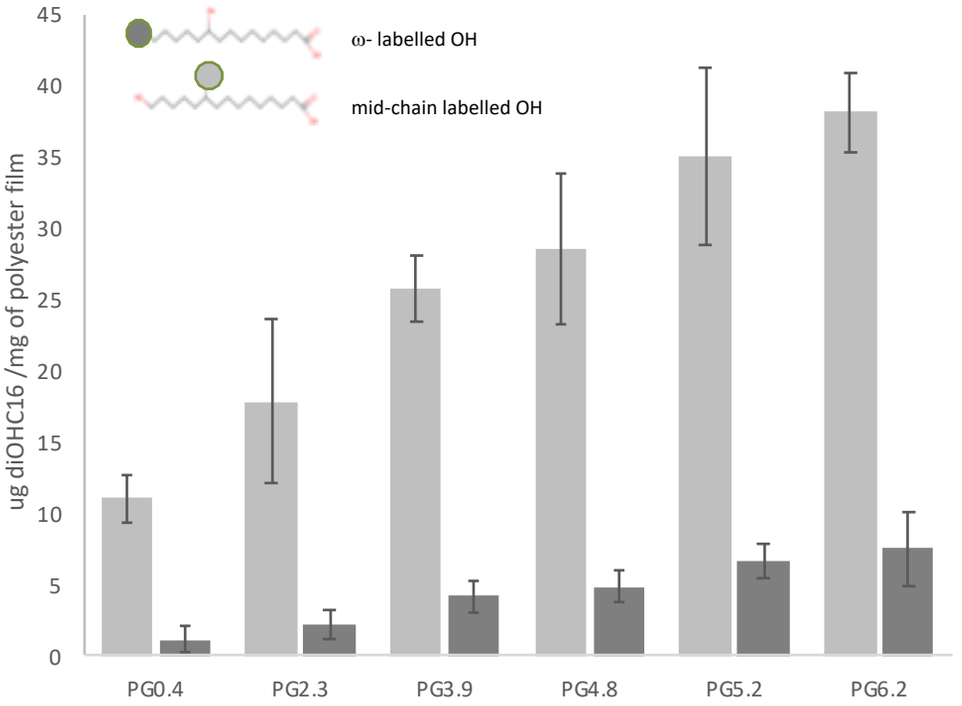

Figure 3. Relative proportion of free OH groups at the ω- and mid-chain position of the the diOHC16 in the co-polyester films.
Values are means of at least three replicates bars are standard deviations

317

318

319 According to the chemical structure of the diOHC16, both, linear and branched ester bonds, can be
320 formed in the co-polyesters. After complete depolymerization, the release of diOHC16 containing labeled
321 OH groups either in ω-position or in midchain-position was compared in the different co-polyesters. In
322 PG0.4, the ratio of labeled mid-chain OH/ω-OH labeled in diOHC16 was around 9, which indicates that the
323 primary OH groups in the ω–position were preferentially esterified compared to the OH groups in the
324 midchain position. This result agrees with the NMR data (**Figure 2B**) and the previous studies of
325 polycondensation of polyhydroxylated fatty acids (Benitez et al., 2015). A similar ratio was previously

reported for tomato fruit cutin (Philippe et al., 2016). Furthermore, taking PG0.4 as a reference, the gradual introduction of glycerol in the co-polyesters resulted in a gradual increase (up to 3.5-fold) in the labeled OH groups, in particular in the midchain position. These results indicate that the introduction of glycerol in the co-polyesters induced a gradual decrease in the esterification of midchain hydroxyl groups involved in ester bonds and an increase in the linear polymerization scheme within the co-polyesters.

3.3. Glycerol content modulates the microstructure and thermo-mechanical properties of the co-polyesters

The thermal properties of all the produced co-polyesters were investigated by DSC on heating from -50°C to 80°Cat 3°C.min^{-1}. Characteristic thermograms are superimposed in **Figure 4A**. We checked that the cooling step at -50°C did not modify the crystallinity of the samples. The thermograms of the co-polyesters exhibited various events as a function of the composition, i.e., the amount of esterified glycerol in the samples. From -30°C to 0°C, depending on the glycerol content, the baseline fall was attributed to the glass transition characterizing the amorphous phase of the co-polyesters. The glass transition temperatures (Tg), determined at the midpoint of the baseline fall, were determined for each co-polyester (**Table 1)**. The Tg value determined for the PG0.4 sample containing only traces of glycerol is -8.7°C, similar to that measured on polyester catalyst- produced (-7°C) from hydroxy fatty acids extracted from green tomato cutin (Benitez et al., 2015). Interestingly, the Tg significantly decreased from -8.7 to -20.4°C with the gradual introduction of glycerol (up to 6.2% wt.) within the co-polyesters, suggesting that the mobility of the co-polyester chains increased giving rise to a more relaxed structure. This result is consistent with the observed reticulation pattern of the co-polyesters (**Figure 3**).

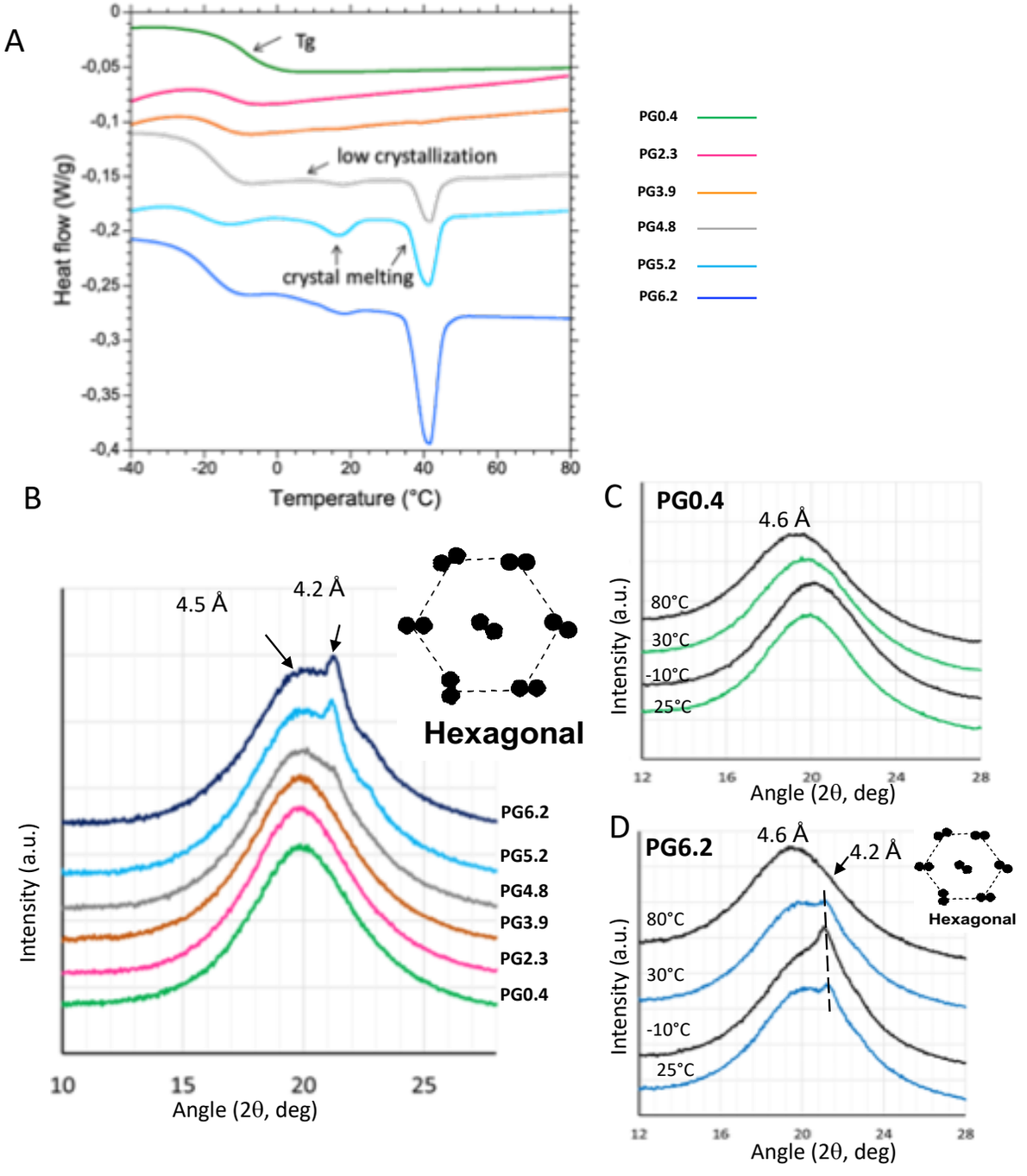

Figure 4. DSC and XRD analyses of the different cutin-like diOHC16-glycerol co-polyester films

A . DSC thermogram of the different co-polyesters containing increasing level of glycerol from 0.4 % wt (for PG0.4) to 6.2% wt (for PG6.2). **B**, XRD patterns of the different co-polyesters recorded at 25°C.**,** XRD patterns recorded for PG0.4 (**C**) and PG6.2 (**D**) at different temperatures.

348

349 For the co-polyesters containing glycerol amounts lower than 4% wt. (PG0.4, PG2.3, PG3.9), the DSC

thermograms recorded on heating did not exhibit thermal events above 0°C (**Figure 4A)**. However, for the co-polyesters containing higher amounts of glycerol (PG4.8, PG5.2, and PG6.2), endothermic events were recorded and related to the gradual incorporation of glycerol in the materials. Indeed, for these co-polyesters, two successive endothermic peaks were recorded around 17°C and 40°C. These endotherms may correspond to structural reorganizations, and/or changes in the physical state of molecules in the co-polyesters. The second endothermic peak (40°C) exhibits a higher enthalpy than the first, and increases with the level of glycerol content (**Table 1**).

The X-ray diffraction experiments performed at 25°C showed at wide angles a bump centered at 2θ=19° (d=4.5 Å), corresponding to the amorphous state of the co-polyesters (**Figure 4B**). In the co-polyesters containing at least 5 % wt. of glycerol (PG5.2, PG6.2), a peak at 2θ=21.2° was recorded (**Figure 4B**). This peak corresponds to a repeat distance of 4.2 Å between the acyl chains which is characteristic of a hexagonal packing of acyl chains. This single peak constitutes the XRD signature of the formation of a crystalline organization of the linear esterified acyl chains within the co-polyesters containing at least 5% wt. glycerol. This XRD peak was superimposed to the bump centered at 4.5 Å (**Figure 4B**), which corresponds to the coexistence of crystalline and amorphous states within the co-polyesters. The presence of glycerol in the samples, and the esterification occurring between the hydroxyl groups of glycerol (mainly in *sn-1* and *sn-3* positions) and the carboxyl groups of the fatty acids induced a linear organization of the chains or the formation of shorter chains. This spatial proximity between the linear and shorter co-polyester chains may favor short-distance hydrophobic interactions between the acyl chains and result in a crystalline organization with a hexagonal packing below the melting temperature of the fatty acids. In absence of glycerol, the reticulation involves the hydroxyl groups both in midchain hydroxyl and ω-

positions. This prevents short-distance hydrophobic interactions between the linear chains formed by primary esterification, hence avoiding the formation of a crystalline organization in the co-polyesters.

The thermotropic phase behavior of the co-polyesters formed with very low (PG0.4) or high (PG6.2) amount of glycerol, were investigated by XRD at various temperatures ranging from -10°C to 80°C that have been selected according to the DSC results (**Figure 4A**). In presence of very low glycerol content (**Figure 4C**), the amorphous state of the polyester was characterized by a bump of RX diffusion, centered in a mean value that was affected by the temperature. The increase of temperature induced a shift toward lower angle values corresponding to higher distances between the acyl chains associated with an increase in the molecular mobility. In the presence of 6 % wt. of glycerol (**Figure 4D**), the XRD experiments were conducted at 25°C, then the samples were cooled to -10°C, heated to 30°C (i.e., above the first endotherm) and then finally to 80°C (i.e., above the second endotherm). The single peak at 2θ=21.2° (4.2 Å) was recorded at 25°C, confirming the results previously obtained. Decreasing the temperature to -10°C increased the intensity of the XRD peak at 2θ=21.2° related to a hexagonal phase and was interpreted as an increase in the amount of the crystalline phase formed in the co-polyesters. On heating at 30°C, the intensity of the XRD decreased. Increasing the temperature at 80°C, i.e., above the second endotherm recorded by DSC and then above the melting point of the crystalline structures, induced the disappearance of the XRD peak at 2θ=21.2°and to the recording of an XRD bump centered at 4.6 Å characteristic of acyl chains in a melted state. These XRD experiments evidenced the temperature-dependent behavior of the co-polyester, with the presence of various amounts of hexagonal phase as a function of temperature.

The two endotherms revealed successively by DSC correspond to independent packing events of the molecules both organized in a hexagonal form as revealed by XRD. The different melting temperatures may correspond to packing of molecules with various compositions, *e.g*. chain length.

393 The thermo-mechanical behavior of all co-polyesters was analyzed by DMTA. **Figure 5A** shows the
394 plot of the storage modulus (E') and the loss factor tan δ of the co-polyesters. For all samples, the large
395 peak of tan δ corresponds to the main mechanical relaxation α which is associated with the calorimetric
396 glass transition from a glassy to a rubbery state. The relaxation temperature from the glassy to the rubbery
397 state (T_α), determined at the maximum of the tan δ curve, decreases from 8.6°C to 0.2°C when glycerol
398 content increases (**Table 1**). In agreement with the T_g values obtained by DSC analyses (**Table 1**) such a
399 depressor effect of glycerol on T_α further strengthens the impact of glycerol on the properties of the cutin-

400 like co-polyesters.

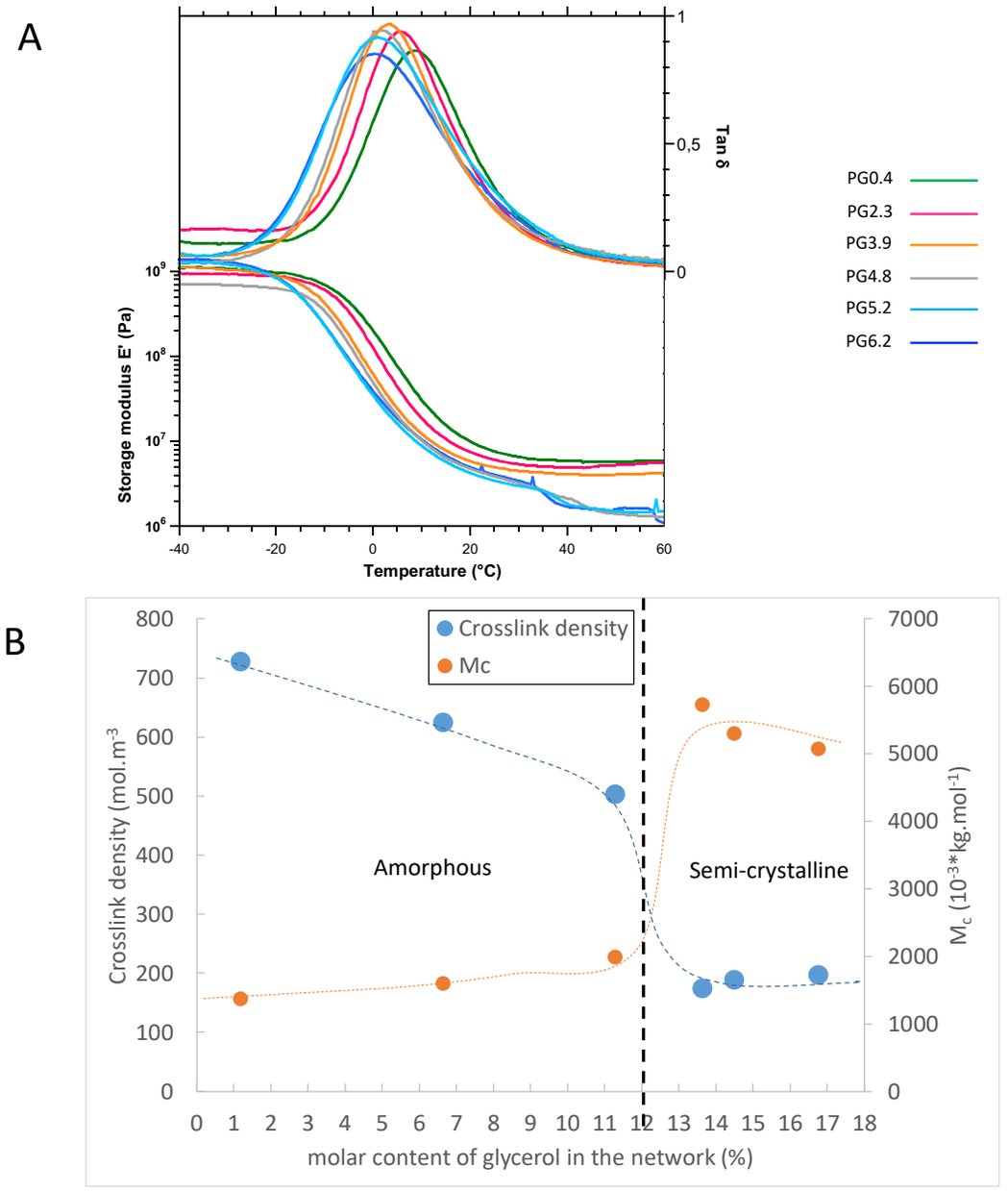

Figure 5 – DMA analysis of the cutin-like diOHC16-glycerol co-polyesters

A – Plot of the storage modulus (E') and the loss factor tan δ of the co-polyesters with different level of esterified glycerol content.
B- Evolution of the crosslink density and the average mass between crosslinks as a function of the molar content of glycerol in the network. Dashed lines are just guides for the eyes.

401

A second event appears on storage modulus which slightly falls in the temperature range 30-40°C for the composition containing more than 4% (wt.) of glycerol (PG4.8, PG5.2, PG6.2) (**Figure 5A**). This transition is attributed to the melting of the crystalline phase according to DSC and XRD results (**Figure 4**). Finally, the plateau of storage modulus is reached at about 50°C with a value which decreases from 5.867 MPa to 1.589 MPa when glycerol content increases from 0.4 to 6% wt. (**Table 1**).

These values are typical of rubber elasticity suggesting an elastomeric behavior of the co-polyesters. This was confirmed by the tensile tests performed at room temperature. The tensile strength, strain at break and, Young Modulus are reported in **Table1**, and the characteristic curves are plotted in **Figure 6**.

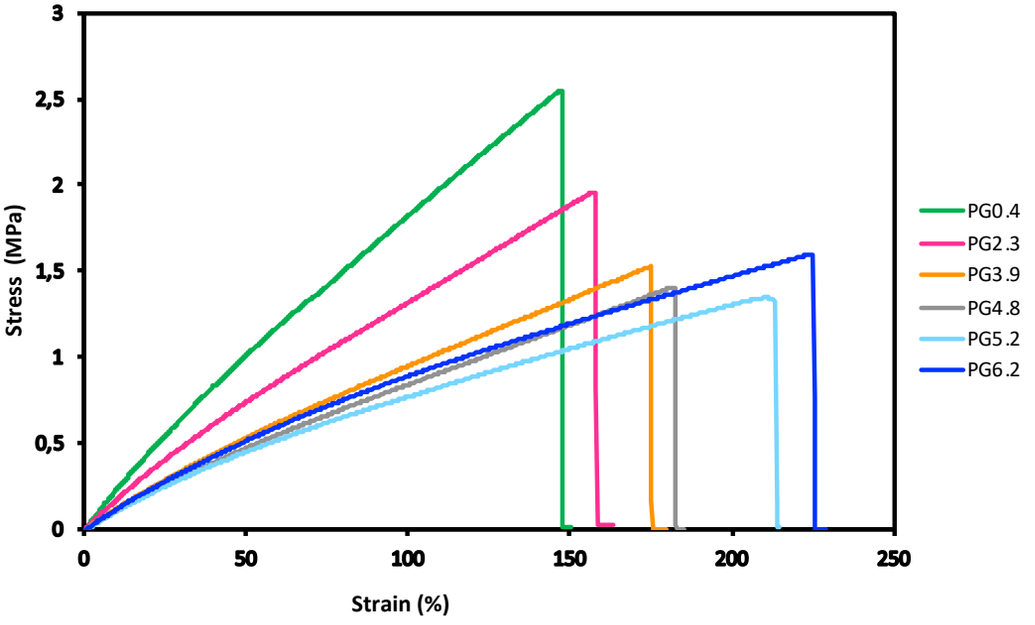

Figure 6- Typical Stress-strain curves of the cutin-like diOHC16-glycerol co-polyester films from 0.4 % wt. for PG0.4 to 6.2% wt. for PG6.2

All films, either with low or high glycerol contents, show a quasi-linear and reversible stress-strain behavior with high elongation at break (> 100%) comparable to synthetic elastomers. It is striking that after

breakage, the dogbone tensile test specimens show a complete elastomeric recovery of their initial shape (Supplemental Figure 2). The mechanical properties of the PG0.4 are comparable to those previously described for other polyhydroxylated fatty acid-based polyesters (Benitez et al., 2015; Benítez et al., 2015). Moreover, our present data show that the mechanical properties were strongly modified by the gradual introduction of glycerol in the co-polyesters which resulted in a decrease in the Young modulus (from 2.29 to 1. 19 MPa), as well as in the stress at break (from 2.1 to 1.5 MPa). Surprisingly, higher glycerol of 6% induces a slight increase of tensile strength simultaneous to the increase of strain at break. It is certainly due to the crystallinity evidenced by calorimetry and XRD measurements (Figure 4).

The most striking observation is the increase in strain at break from 124% to 217 % (for PG0.4 and PG6.2 respectively) induced by the esterified glycerol in the co-polyesters **(Table1, Figure 6**). This elongation value is comparable to some synthetic rubber such as ethylene-propylene-diene or polysulfide-butadiene rubbers (Shanks and Kong, 2013). This strain at break induced by a higher glycerol/hydroxy fatty acid ratio fully fits the CUS1 tomato phenotype which is affected in cutin deposition(Philippe et al., 2016). Importantly, the CUS1 tomato cutin polyester exhibited a fivefold increase in the glycerol ratio (vs hydroxy fatty acids), which probably account for the increase in its extensibility and the absence of cracks observed on the CUS1 fruits, regardless that their cuticle density shows a threefold reduction (Girard et al., 2012).

Since our co-polyesters behave like elastomers displaying rubber elasticity, the Flory theory (Flory, 1953) may bring information about the macromolecular structure of the networks (Tran et al., 2018). Accordingly, the crosslink density ν (mole.m^{-3}) is given by:

$$\nu = \frac{E}{3RT} \qquad \text{(equation 2)}$$

Where: R is the gas constant 8.32 J.mol^{-1}.K^{-1}, T is the temperature in Kelvin, and E the elastic modulus at small deformation. This model assumes that the material is amorphous and consequently, we will use the plateau storage modulus values measured in DMTA at 50°C (T = 323 K, that is to say above the melting point of the semi-crystalline samples.).

Therefore, the average molecular mass *Mc* (kg.mol^{-1}) of elastically active chains between crosslinks is:

$$M_c = \frac{3RT\rho}{E} \qquad \text{(equation 3)}$$

Where: ρ is the density of the material in Kg.m^{-3}. The density of the co-polyesters at 50°C could not be measured. As a first approximation, we considered a constant density ρ= 1000 kg.m^{3} for the calculations reported in **Table 2 and Figure 5B.**

	n	$M_{c\ (g/mol)}$	M_c/M_0	Esterified molar glycerol content *
	(mol.m^{-3})	(10^{-3} kg.mol^{-1})	-	mol %
PG 0.4	728	1374	5.1	1.2
PG 2.3	625	1601	5.9	6.64
PG 3.9	503	1987	7.4	11.3
PG 4.8	175	5726	21.2	13.6
PG 5.2	189	5301	19.6	14.5
PG 6.2	197	5074	18.8	16.8

* the molar content of glycerol in the networks given by

$$esterified\ Glycerol\ (mol\%) = \frac{\frac{esterified\ glycerol\ w\%}{M_{glycerol}}}{\frac{esterified\ glycerol\ w\%}{M_{glycerol}} + \frac{(100 - free\ glycerol\ w\% - esterified\ glycerol\ w\%)}{M_{diOH16}}}$$

Table 2 : Macromolecular structure of the network predicted by the Flory theory

PG0.4, PG2.3, and PG3.9 show the largest crosslink density values in the range of 500- to 730 mol.m^{-3} associated with small values of M_c in the 1300-2000 g.mol^{-1} range. Concurrently, much lower values of ν (175 to 200 mol.m^{-3}) are obtained for samples PG4.8, PG5.2, and PG6.2, with higher values of M_c in the 5000-5700 g.mol^{-1} range.

In a first approximation, the number of polymerized diOHC16 repeating units between crosslinks can be estimated by dividing these values of M_c by a repeating unit mass M_o= 270 g.mol^{-1} (this value assumes that elastically active chains consist essentially of polymerized diOHC16 monomer units in which only 1 acid and 1 hydroxyl group have reacted.)

The values of the ratio M_c/M_o calculated in **Table 2** suggest that for samples PG0.4, PG2.3, and PG3.9 the number of polymerized diOHC16 repeating units should range from 5 to 7, while 19 to 21 repeating units are predicted for samples PG4.8, PG5.2, and PG6.2. For the latter, a few glycerol units are probably also present in the elastically active chains. Anyhow, such a loosening of the network induced by the gradual introduction of the glycerol is in full accordance with the increase in the labeling of free OH groups within the co-polyesters (**Figure 3**).

Besides, the plot of ν and M_c as a function of this molar content of glycerol chemically bound to the network is shown in Figure 5B. A sharp transition from dense amorphous networks (PG0.4, PG2.3, and PG3.9) to loose semi-crystalline networks (PG4.8, PG5.2, and PG6.2) seems to take place around a threshold value of 12 mol% of glycerol.

The development of crystallinity for higher glycerol contents may be ascribed to the flexibility of the long-chain segments between two crosslinks which become able to fold into crystallites, while at lower glycerol content the shorter chains remain amorphous.

3.4. Glycerol can modify the barrier properties of the co-polyesters and their interaction with bacterial cells

469 Water permeance and oxygen barrier properties of the co-polyesters were analyzed. All the produced co-
470 polyesters showed low water vapor permeance properties (**Figure 7A**) around 10^{-9} $m.s^{-1}$, in the same range
471 as the plant cuticle permeance and some synthetic membrane, such as 3μm parafilm or 3μm polyethylene
472 (Valeska Zeisler-Diehl et al., 2017). The introduction of esterified glycerol and the associated modification
473 of the branching of the co-polyesters induced a slight, but statistically not significant, increase in the water
474 vapor permeability of the co-polyesters. This result is consistent with our previous data showing that a
475 modification of the polymerization index did not significantly impact the water permeance of tomato
476 cutins (Philippe et al, 2016).

A

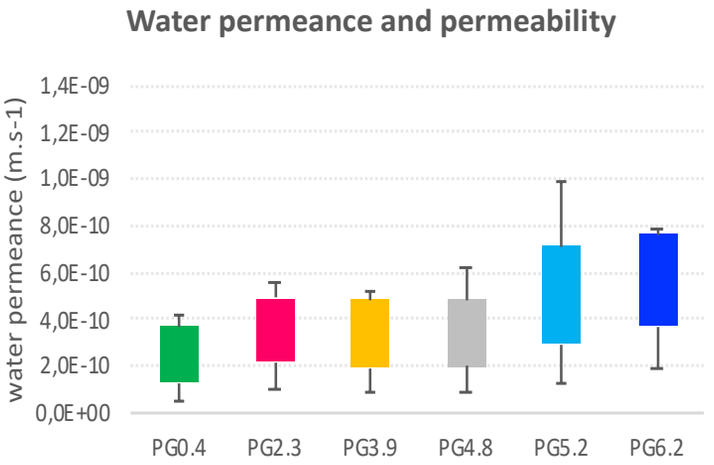

B

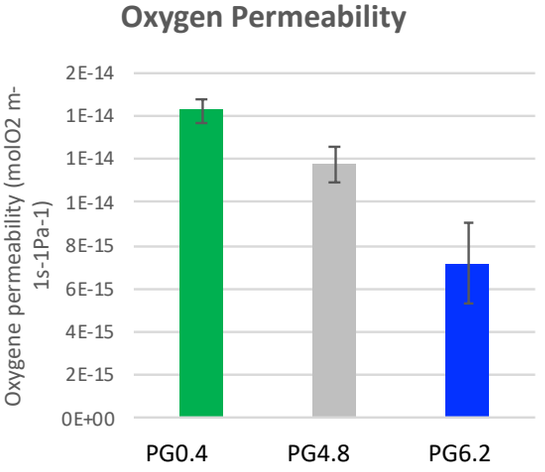

Figure 7- Barrier properties of the cutin-like co-polyesters
Water permance (A) and Oxygen (B) barrier properties of the cutin-like diOHC16-glycerol co-polyesters containing increasing level of glycerol (0.4 %wt for PG0.4 to 6.2% wt for PG6.2)

The oxygen permeability of the cutin-derived co-polyesters ranged between 0.7 and 1.4 x 10^{-14} mol m^{-1} s^{-1} Pa^{-1} (Figure 7B). These values are in the same order of magnitude as synthetic polymers commonly used for food packaging such as low-density polyethylene (0.1-0.2 x 10^{-14} mol.m^{-1}.s^{-1}.Pa^{-1}) (Durmuş et al., 2007; Matar et al., 2018; Motedayen et al., 2019). These values are also comparable to polylactic acid (PLA), a bio-based polyester, for which oxygen permeability values ranging between 1x10^{-16} and 1x10^{-14} mol. m^{-1}.s^{-1}.Pa^{-1} have been reported (Lehermeier et al., 2001; Mahmoodi et al., 2019; Palai et al., 2019).

Other polyesters such as fossil-based polyethylene terephthalate, or microbial synthesized polyhydroxyalkanoates (PHAs) have considerably higher barrier properties with oxygen permeability in the order of $1x10^{-17}$ mol m^{-1} s^{-1} Pa^{-1} (Ambrosio-Martin et al., 2016; Crétois et al., 2014).

Interestingly, increasing the ratio of esterified glycerol in the co-polyesters improved the oxygen barrier properties of the films by reducing oxygen permeability by half (**Figure 7B**). This is probably associated with the increase of crystallinity, as observed for other elastomers (Wang et al., 2012) reducing the motion needed for oxygen diffusion.

Finally, the antibacterial activity of the co-polyesters containing the lowest and the highest levels of esterified glycerol (PG0.4 and PG6.2) was assessed on *E. coli* and *S. aureus*. After exposure to the co-polyester films, no labeling of dead cells was revealed (**Figure 8A**), which indicates that the co-polyesters were devoid of bactericidal properties regardless of the glycerol content. This result contrasts with the biocide activity that was demonstrated with acyl glycerol esters of hydroxy fatty acids (Correia et al., 2020) or with films formed by self-assembly of these esters (Ferreira et al., 2014; Garcia et al., 2010) extracted by an ionic liquid catalyst from suberin, another hydrophobic plant polyesters.

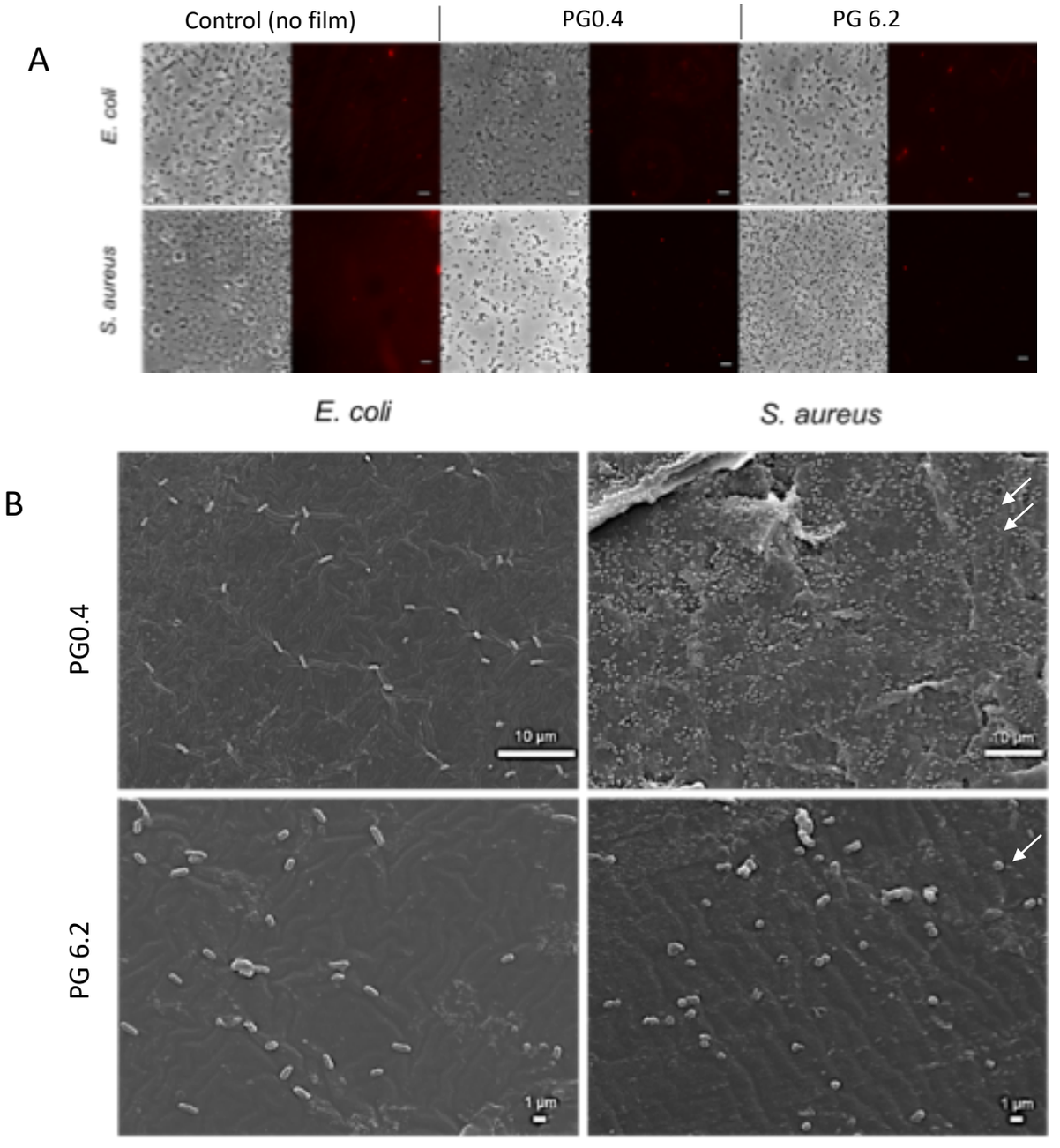

Figure 8. Microscopy imaging of the cutin-like co-polyesters PG0.4 and PG6.2 after incubation with *E. coli* and *S. aureus*.

A. Co-polyesters films activity against *E. coli* and *S. aureus*. Following exposure of bacteria to films pieces their morphology and viability were visualized by phase-contrast and fluorescence microscopy using Texas Red filter (dead cells are revealed by red fluorescence due to propidium iodide labelling), respectively. Controls was conducted without films. The scale bar in all images is 5µm.

B. Cells adherent onto the surface of the cutin co-polyester films were observed by SEM microscopy. No differences were noticed in the numbers of adherent *E. coli* cells in either co-polyester films. Conversely, the number of *S. aureus* adherent cells (ex under arrows) are significantly higher in the PG0.4 co-polyester compared to the PG6.2. The scale bar in all images is shown at the bottom.

498

Since the co-polyesters are devoid of bactericidal capacity, we further analyzed the films' surface following their incubation with bacteria (**Figure 8 B**). For either co-polyester, the numbers of adherent *E. coli* cells were low and comparable. Remarkably over the surface of the PG0.4 co-polyester, *S. aureus* formed a compacted biofilm whereas PG6.2 hinder significantly the adhesion of this bacteria species. This result demonstrates that increased glycerol levels in the cutin-inspired co-polyesters lead to a significant reduction of bacterial fouling. (**Figure 8 B**). The observed differences between the two bacteria species might be due to the electronegativity of the cells surface that is higher in *E. coli* than *S. aureus*, regardless that their different morphologies and surface roughness (rods and cocci, respectively) may greatly influence their adhesion in the conditions used here. This observation, supported by the structural, thermal, and mechanical analyses, suggests that glycerol esterification altered the smoothness of the films' surface as well as their surface charge. One important finding is that by increasing further the glycerol levels in the cutin co-polyesters their anti-biofouling properties can be potentiated.

4. Conclusions

We report in this work, the production of glycerol/hydroxy fatty acid co-polyesters by a catalyst- and solvent-free polycondensation process. Glycerol and hydroxy fatty acids are biosourced molecules from by-products and wastes produced by the oilseed and tomato processing industries, respectively. These co-polyesters elastomers obtained are 100% biobased and bioinspired by the cutin polymer of plant cuticles, which is also composed of hydroxy-fatty acids and glycerol. Drawing on our previous studies on tomato fruit cuticle, we gradually increased the glycerol content while remaining in a concentration range observed in most plant cuticles. The co-polyesters obtained are insoluble and displayed tensile mechanical

behavior comparable to that of some synthetic elastomers. By adjusting the level of esterified glycerol, we induced modifications of the reticulation pattern which was associated with variation in chain mobility and extensibility. Glycerol also induced the loosening of the elastically active chain network and the formation of crystalline domains. These modifications were associated with variations in the tensile mechanical and barrier properties of the co-polyesters as well as the adhesion of microorganisms.

The exact macromolecular structure of the co-polyesters probably involves not only glycerol and diOHC16 but also minor components present in the fatty acid extract. The elucidation of the role in the reaction scheme will be the subject of future work. Indeed, these hydroxy fatty acid/glycerol co-polyesters provide excellent templates to further delineate the relationships between the complex molecular and macromolecular architecture and the functional properties of plant cuticular barriers. This bioinspired approach also allows developing green polymer composites adapted to specific applications for food, packaging industry, or as an antifouling natural product. Furthermore, increasing the contents of glycerol led to available free hydroxyl groups for grafting and covalent substitutions for tailored functionalization, opening new routes for high-value applications (e.g., in the medical sector).

Figure Caption

Figure 1 – Solvent- and catalyze-free polycondensation of tomato cutin extract and glycerol

Figure 2 – ATR-FTIR and NMR spectra of the cutin-like polyesters films

A . ATR-FTIR spectra of hydroxy fatty acid (diOHC16) extracted from tomato cutin and the corresponding polymers with high (PG6.2) or low (PG0.4) glycerol. In the inset, the magnification of the C=O stretching bands at 1715 cm^{-1} and 1733 cm^{-1} are assigned to the ester group, involved or not in hydrogen bonds, respectively, whereas the vibration at 1703 cm^{-1} is assigned to the carboxylic group.

B. Solid-State ^{13}C CP-MAS NMR spectra of the polymers

Figure 3- Relative proportion of free OH groups at the ω- and mid-chain position of the diOHC16 in the co-polyester films.

Values are means of at least three replicates bars are standard deviations

Figure 4- DSC and XRD analyses of the different cutin-like diOHC16-glycerol co-polyester films

A, DSC thermogram of the different co-polyesters containing increasing levels of glycerol from 0.4 % wt (for PG0.4) to 6.2% wt (for PG6.2). **B**, XRD patterns of the different co-polyesters recorded at 25°C. XRD patterns for PG0.4 (**C**) and PG6.2 (**D**) recorded at different temperatures.

Figure 5- DMA analysis of the cutin-like diOHC16-glycerol co-polyesters

A – Plot of the storage modulus (E') and the loss factor tanδ of the co-polyesters with different levels of esterified glycerol content.

B- Evolution of the crosslink density and the average mass between crosslinks as a function of the molar content of glycerol in the network. Dashed lines are just a guide for the eye.

Figure 6- Typical Stress-strain curves of the cutin-like diOHC16-glycerol co-polyester films from 0.4 % wt. for PG0.4 to 6.2% wt. for PG6.2

Figure 7- Barrier properties of the cutin-like co-polyesters

564 Water permeance (A) and oxygen (B) barrier properties of the cutin-like diOHC16-glycerol co-polyesters
565 containing increasing levels of glycerol (0.4 %wt for PG0.4 to 6.2% wt for PG6.2)
566
567 **Figure 8- Microscopy imaging of the cutin-like co-polyesters PG0.4 and PG6.2 after incubation with *E. coli* and *S.***
568 ***aureus*.**
569 **A.** Co-polyesters films activity against *E. coli* and *S. aureus*. Following exposure of bacteria to film pieces,
570 their morphology and viability were visualized by phase-contrast and fluorescence microscopy using Texas
571 Red filter (dead cells are revealed by red fluorescence due to propidium iodide labelling), respectively.
572 Controls were conducted without films. The scale bar in all images is 5µm.
573 **B.** Cells adherent onto the surface of the cutin co-polyester films were observed by SEM microscopy. No
574 differences were noticed in the numbers of adherent *E. coli* cells in either co-polyester films. Conversely,
575 the number of *S. aureus* adherent cells (ex under arrows) are significantly higher in the PG0.4 co-polyester
576 compared to the PG6.2. The scale bar in all images is shown at the bottom.
577
578 **Supplemental Figure 1- Composition and characterization of the cutin monomer extracted from tomato cutin**
579 **from industrial tomato peels**
580 A. Cutin monomer composition. Values are means (standard deviation) of three experiments. B. FTIR
581 spectrum. C. UV spectrum
582
583 **Supplemental Figure 2- Elastomeric recovery cutin-inspired polyesters.**
584 On the left, an image of the elastomeric sample (PG0.4) before and after a mechanical test (right) showing
585 its total shape recovery

Acknowledgment

This work was supported by an INRAE Transfer grant (ELASTOMAT project) and the INRAE TRANSFORM department. RR is grateful to FCT funding for his Ph.D. scholarship (SFRH-BD-110467-2015).

The authors thank André Lelion for his technical assistance.

References

Aleixandre-Tudo, J.L., du Toit, W., 2018. The role of UV-visible spectroscopy for phenolic compounds quantification in winemaking, in: Solis-Oviedo, R.L., dela Cruz Pech-Canul, A. (Eds.), Frontiers and new trends in the science of fermented food and beverages. https://doi.org/DOI:10.5772/intechopen.79550

Ambrosio-Martin, J., Fabra, M.J., López-Rubio, A., Gorrasi, G., Sorrentino, A., Lagaron, J.M., 2016. Assessment of ball milling as a compounding technique to develop nanocomposites of poly(3-hydroxybutyrate-co-3-hydroxyvalerate) and bacterial cellulose nanowhiskers. J. Polym. Environ. 24, 241-254.https://doi.org/10.1007/s10924-016-0767-6

Barker, J.C., 1988. Russeting (cuticle cracking) in glasshouse tomatoes in relation to fruit growth. J. Hortic. Sci. 63, 459-463.https://doi.org/10.1080/14620316.1988.11515879

Benítez, J.J., Castillo, P.M., Del Río, J.C., León-Camacho, M., Domínguez, E., Heredia, A., Guzmán-Puyol, S., Athanassiou, A., Heredia-Guerrero, J.A., 2018. Valorization of tomato processing by-products: fatty acid extraction and production of bio-based materials. Materials (Basel) 11.https://doi.org/10.3390/ma11112211

Benitez, J.J., Heredia-Guerrero, J.A., Guzman-Puyol, S., Barthel, M.J., Dominguez, E., Heredia, A., 2015. Polyhydroxyester films obtained by non-catalyzed melt-polycondensation of natural occurring fatty polyhydroxyacids. Front. Mater. 2, 10.https://doi.org/10.3389/fmats.2015.00059

Benítez, J.J., Heredia-Guerrero, J.A., Guzmán-Puyol, S., Domínguez, E., Heredia, A., 2015. Long-chain polyhydroxyesters from natural occurring aleuritic acid as potential material for food packaging. Soft Mater. 13, 5-11.https://doi.org/10.1080/1539445X.2014.993476

Cogognigni, I., Montanari, A., de la Torre Carreras, R., Cardoso Bernet Montserrat, G., 2014. Extraction method of a polyester polymer or cutin from the wasted tomato peels and polyester polimer so extracted

Correia, V.G., Bento, A., Pais, J., Rodrigues, R., Haliński, Ł.P., Frydrych, M., Greenhalgh, A., Stepnowski, P., Vollrath, F., King, A.W.T., Silva Pereira, C., 2020. The molecular structure and multifunctionality of the cryptic plant polymer suberin. Materials Today Bio 5, 100039.https://doi.org/10.1016/j.mtbio.2019.100039

Crétois, R., Follain, N., Dargent, E., Soulestin, J., Bourbigot, S., Marais, S., Lebrun, L., 2014. Microstructure and barrier properties of PHBV/organoclays bionanocomposites. J. Membrane Sci. 467, 56-66.https://doi.org/10.1016/j.memsci.2014.05.015

Durmuş, A., Woo, M., Kaşgöz, A., Macosko, C.W., Tsapatsis, M., 2007. Intercalated linear low density polyethylene (LLDPE)/clay nanocomposites prepared with oxidized polyethylene as a new type compatibilizer: Structural, mechanical and barrier properties. Eur. Polym. J. 43, 3737-3749.https://doi.org/10.1016/j.eurpolymj.2007.06.019

Fameau, A.-L., Gaillard, C., Marion, D., Bakan, B., 2013. Interfacial properties of functionalized assemblies of hydroxy-fatty acid salts isolated from fruit tomato peels. Green Chem. 15, 341-346.https://doi.org/10.1039/C2GC36677K

Feast, W.J., Stainton, N.M., 1995. Synthesis, structure and properties of some hyperbranched polyesters. Journal of Materials Chemistry 5, 405-411.https://doi/10.1039/JM9950500405

Ferreira, R., Garcia, H., Sousa, A.F., Guerreiro, M., Duarte, F.J.S., Freire, C.S.R., Calhorda, M.J., Silvestre, A.J.D., Kunz, W., Rebelo, L.P.N., Silva Pereira, C., 2014. Unveiling the dual role of the cholinium hexanoate ionic liquid as solvent and catalyst in suberin depolymerisation. RSC Advances 4, 2993-3002.https://doi.org/10.1039/C3RA45910A

Fich, E.A., Segerson, N.A., Rose, J.K., 2016. The plant polyester cutin: biosynthesis, structure, and biological roles. Annu. Rev. Plant Biol. 67, 207-233.https://doi.org/10.1146/annurev-arplant-043015-111929

Flory, J.P., 1953. Elasticity of rubber, Principles of Polymer Chemistry, Ithaca, N.Y. : Cornell University Press ed. https://doi.org/DOI:10.1126/science.119.3095.555-a.

Fritsch, C., Staebler, A., Happel, A., Cubero Márquez, M.A., Aguiló-Aguayo, I., Abadias, M., Gallur, M., Cigognini, I.M., Montanari, A., López, M.J., Suárez-Estrella, F., Brunton, N., Luengo, E., Sisti, L., Ferri, M., Belotti, G., 2017. Processing, valorization and application of bio-waste derived compounds from potato, tomato, olive and cereals: A Review. 9, 1492.https://doi.org/doi:10.3390/su9081492

Garcia, H., Ferreira, R., Petkovic, M., Ferguson, J.L., Leitão, M.C., Gunaratne, H.Q.N., Seddon, K.R., Rebelo, L.P.N., Silva Pereira, C., 2010. Dissolution of cork biopolymers in biocompatible ionic liquids. Green Chem. 12, 367-369.https://doi.org/10.1039/B922553F

Girard, A.L., Mounet, F., Lemaire-Chamley, M., Gaillard, C., Elmorjani, K., Vivancos, J., Runavot, J.L., Quemener, B., Petit, J., Germain, V., Rothan, C., Marion, D., Bakan, B., 2012. Tomato GDSL1 is required for cutin deposition in the fruit cuticle. Plant Cell 24, 3119-3134.https://doi.org/10.1105/tpc.112.101055

Graça, J., Schreiber, L., Rodrigues, J., Pereira, H., 2002. Glycerol and glyceryl esters of omega-hydroxyacids in cutins. Phytochemistry 61, 205-215.https://doi.org/10.1016/s0031-9422(02)00212-1

Heredia-Guerrero, J.A., Benítez, J.J., Domínguez, E., Bayer, I.S., Cingolani, R., Athanassiou, A., Heredia, A., 2014. Infrared and Raman spectroscopic features of plant cuticles: a review. Front. Plant Sci. 5, 305.https://doi.org/10.3389/fpls.2014.00305

Heredia-Guerrero, J.A., Heredia, A., Dominguez, E., Cingolani, R., Bayer, I.S., Athanassiou, A., Benitez, J.J., 2017. Cutin from agro-waste as a raw material for the production of bioplastics. J. Exp. Bot. 68, 5401-5410.https://doi.org/10.1093/jxb/erx272

Herrera, F., Pulgarin, C., Nadtochenko, V., Kiwi, J., 1998. Accelerated photo-oxidation of concentrated p-coumaric acid in homogeneous solution. Mechanistic studies, intermediates and precursors formed in the dark. Appl. Catal. B-Environ. 17, 141-156.https://doi.org/10.1016/S0926-3373(98)00008-3

Lehermeier, H.J., Dorgan, J.R., Way, J.D., 2001. Gas permeation properties of poly(lactic acid). J. Membrane Sci. 190, 243-251.https://doi.org/10.1016/S0376-7388(01)00446-X

Mahmoodi, A., Ghodrati, S., Khorasani, M., 2019. High-strength, low-permeable, and light-protective nanocomposite films based on a hybrid nanopigment and biodegradable PLA for food packaging applications. ACS Omega 4, 14947-14954.https://doi.org/10.1021/acsomega.9b01731

Matar, C., Gaucel, S., Gontard, N., Guilbert, S., Guillard, V., 2018. Predicting shelf life gain of fresh strawberries 'Charlotte cv' in modified atmosphere packaging. Postharvest Biol. Tec. 142, 28-38.https://doi.org/10.1016/j.postharvbio.2018.03.002

Motedayen, A.A., Rezaeigolestani, M., Guillaume, C., Guillard, V., Gontard, N., 2019. Gas barrier enhancement of uncharged apolar polymeric films by self-assembling stratified nano-composite films. RSC Advances 9, 10938-10947.https://doi.org/10.1039/C9RA01109A

Nawrath, C., 2006. Unraveling the complex network of cuticular structure and function. Curr. Opin. Plant Biol. 9, 281-287.https://doi.org/10.1016/j.pbi.2006.03.001

Palai, B., Biswal, M., Mohanty, S., Nayak, S.K., 2019. In situ reactive compatibilization of polylactic acid (PLA) and thermoplastic starch (TPS) blends; synthesis and evaluation of extrusion blown films thereof. Ind. Crop Prod. 141, 111748.https://doi.org/10.1016/j.indcrop.2019.111748

Philippe, G., Gaillard, C., Petit, J., Geneix, N., Dalgalarrondo, M., Bres, C., Mauxion, J.P., Franke, R., Rothan, C., Schreiber, L., Marion, D., Bakan, B., 2016. Ester cross-link profiling of the cutin polymer of Wild-Type and cutin synthase tomato mutants highlights different mechanisms of polymerization. Plant Physiol. 170, 807-820.https://doi.org/10.1104/pp.15.01620

Philippe, G., Geneix, N., Petit, J., Guillon, F., Sandt, C., Rothan, C., Lahaye, M., Marion, D., Bakan, B., 2020. Assembly of tomato fruit cuticles: a cross-talk between the cutin polyester and cell wall polysaccharides. New Phytol. 226, 809-822.https://doi.org/10.1111/nph.16402

Quispe, C.A.G., Coronado, C.J.R., Carvalho Jr, J.A., 2013. Glycerol: production, consumption, prices, characterization and new trends in combustion. Renew. Sust. Energ. Rev. 27, 475-493.https://doi.org/10.1016/j.rser.2013.06.017

Schreiber L, J, S.n., 2009. Water permeability, Water and solute permeability of plant cuticles. Springer Berlin Heidelberg, Berlin, Heidelberg, pp. 61-123. https://doi.org/DOI:10.1007/978-3-540-68945-4

Shanks, R.A., Kong, I., 2013. General purpose elastomers: structure, chemistry, physics and performance, in: Visakh, P.M., Thomas, S., Chandra, A.K., Mathew, A.P. (Eds.), Advances in Elastomers I: Blends and Interpenetrating Networks. Springer Berlin Heidelberg, Berlin, Heidelberg, pp. 11-45. https://doi.org/10.1007/978-3-642-20925-3_2

Shen, Y., Xu, Z., 2013. An improved GC-MS method in determining glycerol in different types of biological samples. J. Chromatogr. B 930, 36-40.https://doi.org/10.1016/j.jchromb.2013.04.034

Tedeschi, G., Benitez, J.J., Ceseracciu, L., Dastmalchi, K., Itin, B., Stark, R.E., Heredia, A., Athanassiou, A., Heredia-Guerrero, J.A., 2018. Sustainable fabrication of plant cuticle-like packaging films from tomato pomace agro-waste, beeswax, and alginate. ACS Sustain. Chem. Eng. 6, 14955-14966.https://doi.org/10.1021/acssuschemeng.8b03450

Testud, B., Pintori, D., Grau, E., Taton, D., Cramail, H., 2017. Hyperbranched polyesters by polycondensation of fatty acid-based ABn-type monomers. Green Chemistry 19, 259-269.https://doi.org/10.1039/C6GC02294D

Tran, T.-N., Guyomard-Lack, A., Cerclier, C., Humbert, B., Colomines, G., Pilard, J.-F., Deterre, R., Bideau, J.-L., Leroy, E., 2018. Natural rubber-based ionogels. J. Renew. Mater. 6, 251--258.https://doi.org/doi:10.7569/JRM.2017.634174

Valeska Zeisler-Diehl, V., Migdal, B., Schreiber, L., 2017. Quantitative characterization of cuticular barrier properties: methods, requirements, and problems. J. Exp. Bot. 68, 5281-5291.https://doi.org/10.1093/jxb/erx282

Wang, Y., Gupta, M., Schiraldi, D.A., 2012. Oxygen permeability in thermoplastic polyurethanes. J. Polym. Sci. Pol. Phys. 50, 681-693.https://doi.org/10.1002/polb.23053

Yeats, T.H., Rose, J.K., 2013. The formation and function of plant cuticles. Plant Physiol. 163, 5-20.https://doi.org/10.1104/pp.113.222737

A

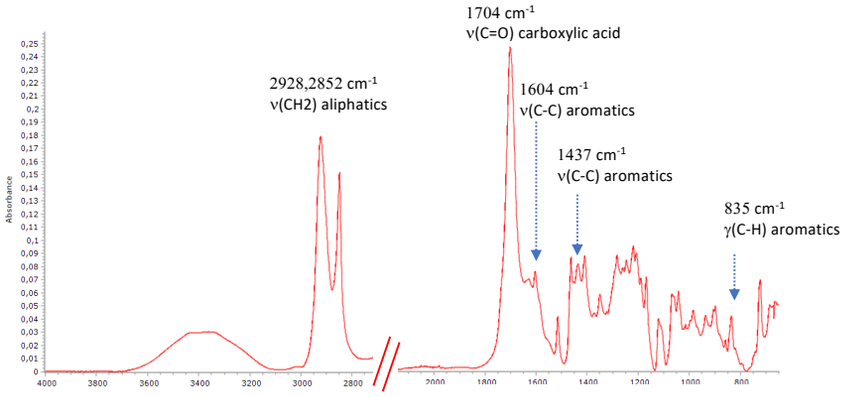

B

cutin monomers batch composition	%	(s.d.)
p-coumaric acid	1.8	(0.3)
16-hydroxy-hexadecanoic acid	2.7	(0.4)
16,9(10)-dihydroxyhexadecanoic acid	92.2	(2.3)
Hexadecane-1,16-dioic acid	0.4	(0.03)
7/8-hydroxy hexadecan-1,16-dioic acid	2.9	(1.2)

C

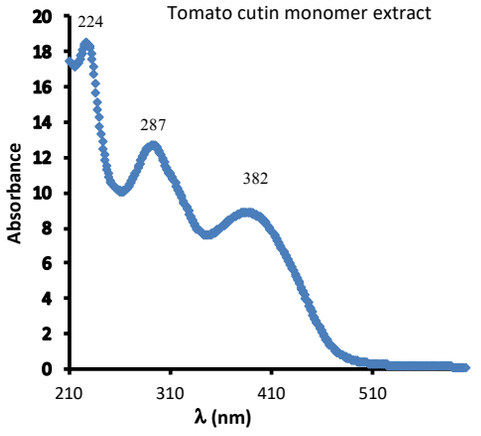

Supplemental Figure 1 – Composition and characterization of the cutin monomer extracted from tomato cutin from industrial tomato peels
A. Cutin monomer composition. Value are means (standard deviation) of three experiments. B. FTIR spectrum. C. UV spectrum

721 303

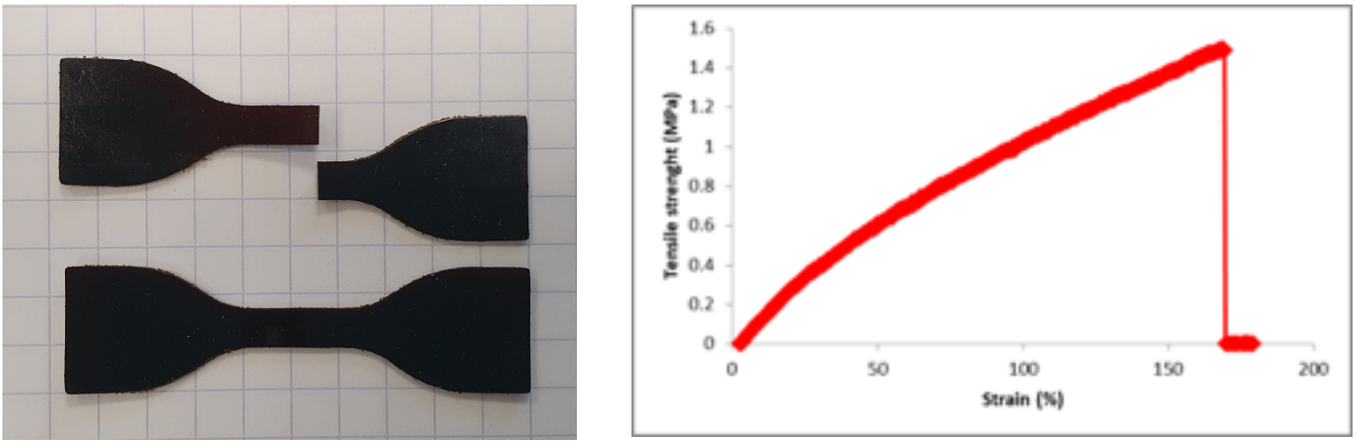

Supplemental Figure 2 – Elastomeric recovery cutin-inspired polyesters

On the left, image of elastomeric sample (PG0.4) before and after mechanical test (right) showing its total shape recovery

722